Published in *Polarization Science and Remote Sensing*,
J. A. Shaw and J. S. Tyo, Eds., Proc. SPIE **5158**, 193–204 (2003)

Polarized light diffusely scattered under smooth and rough interfaces

Thomas A. Germer

Optical Technology Division
National Institute of Standards and Technology
Gaithersburg, MD 20899

ABSTRACT

We develop models for light scattering appropriate for glossy and matte paints. Volume scattering is treated in the single scattering regime and the diffusive scattering regime. In the single scattering regime, scattering is treated in the Rayleigh-Gans approximation, using a Henyey-Greenstein phase function. Interaction of the light with the smooth or rough interface is treated in the facet approximation. The theory for transmissive light scattering by a rough interface in the facet approximation is presented. To treat volume scattering under a rough interface, a Monte Carlo approach is used, where light is allowed to interact with the surface twice, once upon entering the material and once upon exiting. We compare the polarization and intensity predicted by the models with experimental data from glossy and matte paint samples. The results indicate that the new models are an improvement over the Maxwell-Beard model.

Keywords: appearance, coatings, paint, polarization, scatter

1. INTRODUCTION

The development of accurate surface light scattering models based upon first-principles calculations has a variety of applications, including the development of inspection tools for smooth surfaces,[1] the sizing of reference particles,[2,3] the interpretation of remote sensing data,[4] and the modeling of the appearance of automotive coatings.[5] Recent work by our group has indicated that a significant amount of information can be obtained by measuring light scattering polarization.[6-12] While the intensity function is affected by details of the scatterer, such as the power spectral density of surface roughness or the size and shape of a defect, polarization is often a unique signature of the scattering mechanism. For example, polarized light scattering can distinguish rough surfaces from those that scatter by other sources, such as material inhomogeneity, subsurface defects, or particulate contaminants.

Polarized light scattering measurements have attributed the scattering by rough camouflage paint coatings to reflection from the exposed rough interface.[13] The coating had a colored appearance, suggesting that scattering must be at least partially arising from subsurface pigments. It is hard to imagine that dielectric functions of paint materials and the absence of thin dielectric coatings could yield sufficient spectral variation to provide the color of the material. Furthermore, the polarization properties fit the scattering by a rough surface only if the index of refraction of the material were allowed to be unphysically small.

In this article, we investigate the scattering by bulk diffuse scatterers under smooth surfaces and in the presence of surface roughness. The results indicate that much of the polarization signature observed by the scattering by the rough coating can be attributed to subsurface scattering, with the interaction with the rough surface taken into account. The results are more consistent with the observed data.

2. THEORY

In this section, we outline the theory for diffuse scattering under an interface. First, in Sec. 2.1, we describe the polarized phase function that we use for volume scattering. Next, in Sec. 2.2, we use the phase function described in Sec. 2.1 to calculate the singly scattered light under a smooth interface. In Sec. 2.3, we calculate the scattering in the total diffuse limit under a smooth interface. In Sec. 2.4, we calculate the scattering in transmission by a rough surface in the facet approximation. Finally, in Sec. 2.5, we calculate the scattering of a diffuse material under a rough interface, using a Monte Carlo implementation of the theory described in Secs. 2.1, 2.3, and 2.4.

In much of the following, we are concerned with the Mueller matrix probability $\mathbf{P}\,d\Omega$ that a ray traveling from a direction defined by polar angle θ_i and azimuthal angle $\phi_i = \pi$ will scatter into a solid angle $d\Omega$ about a direction defined by polar angle θ_j and azimuthal angle ϕ_j, where *j* is r for reflective scatter and t for transmissive scatter. The Mueller matrix bidirectional scatter distribution function (BSDF) is commonly used to characterize the scatter distribution[14,15] and is defined as

$$\mathbf{f} = \mathbf{P} / \cos\theta_j . \tag{1}$$

The BSDF is often referred to as the bidirectional reflectance distribution function (BRDF) for reflective scatter, and the bidirectional transmittance distribution function (BTDF) for transmissive scatter.

2.1. Polarimetric phase function for single volume scattering

The angular dependence of volume scattering[16] is often characterized in terms of a phase function $p(\theta)$, which describes the probability density that an interaction with the material will result in a ray scattering an angle θ. The phase function, which is normalized to unit probability, is a scalar description of the scattering process and must be adapted to enable its use in a polarimetric context. It is common to employ a generalized phase function to describe the scattering by an arbitrary scatterer, whose properties are not known well enough to provide an *a priori* phase function. By far the most common phase function in the literature is that proposed by Henyey and Greenstein[17] to describe scattering by interstellar dust:

$$p(\theta) = \frac{(1-g^2)}{4\pi(1+2g\cos\theta+g^2)^{3/2}} . \tag{2}$$

The parameter *g* is the average of the cosine of the scattering angle. For $g = 0$, the phase function describes an isotropic scatterer, and as *g* increases, the phase function becomes more strongly peaked in the forward direction. To adapt this function to a polarimetric context, we treat the phase function as a Rayleigh-Gans form factor. We begin by defining a basis set for describing the polarization. If the incident direction is propagating along a unit vector $\hat{\mathbf{k}}_1$, and the scattering direction is along a unit vector $\hat{\mathbf{k}}_2$, then an appropriate basis set in which to describe the scattering matrix is given by the four vectors

$$\hat{\boldsymbol{\sigma}}_1 = \hat{\mathbf{k}}_1 \times \hat{\mathbf{k}}_2 / \left| \hat{\mathbf{k}}_1 \times \hat{\mathbf{k}}_2 \right|, \; \hat{\boldsymbol{\pi}}_1 = \hat{\mathbf{k}}_1 \times \hat{\boldsymbol{\sigma}}_1, \; \hat{\boldsymbol{\sigma}}_2 = \hat{\boldsymbol{\sigma}}_1 , \text{ and } \; \hat{\boldsymbol{\pi}}_2 = \hat{\mathbf{k}}_2 \times \hat{\boldsymbol{\sigma}}_2 , \tag{3}$$

where the vectors with subscript 1 and 2 are used for the incident and scattered light, respectively. We intend to create a phase function whose probability for scattering with unpolarized incident light is given by Eq. (2) and whose polarization properties match that expected from the Rayleigh-Gans approximation. The dyadic relating the incident amplitude to the scattered amplitude is thus assumed to be proportional to the projection dyadic

$$\vec{\mathbf{p}} = \hat{\boldsymbol{\sigma}}_2 \hat{\boldsymbol{\sigma}}_2 + \hat{\boldsymbol{\pi}}_2 \hat{\boldsymbol{\pi}}_2 . \tag{4}$$

The Jones matrix for scattering can be found by applying the basis vectors in Eq. (3) to the dyadic given in Eq. (4):

$$\mathbf{J}_{\text{vol}} = \begin{pmatrix} \hat{\boldsymbol{\sigma}}_2 \cdot \vec{\mathbf{p}} \cdot \hat{\boldsymbol{\sigma}}_1 & \hat{\boldsymbol{\sigma}}_2 \cdot \vec{\mathbf{p}} \cdot \hat{\boldsymbol{\pi}}_1 \\ \hat{\boldsymbol{\pi}}_2 \cdot \vec{\mathbf{p}} \cdot \hat{\boldsymbol{\sigma}}_1 & \hat{\boldsymbol{\pi}}_2 \cdot \vec{\mathbf{p}} \cdot \hat{\boldsymbol{\pi}}_1 \end{pmatrix} = \begin{pmatrix} 1 & 0 \\ 0 & \cos\theta \end{pmatrix}. \tag{5}$$

We choose to normalize the Rayleigh scattering amplitude so that the probability for scattering unpolarized incident light is unity. Therefore, the scattering Mueller matrix is proportional to

$$\frac{2\mathbf{M}(\mathbf{J}_{\text{vol}})}{(1+\cos^2\theta)}, \tag{6}$$

where the function $\mathbf{M}(\mathbf{J})$ represents the Mueller matrix equivalent of a Jones vector $\mathbf{J}$, given in standard texts on the subject.[14,16] We can then adapt the Henyey-Greenstein phase function to polarimetric applications by multiplying Eq. (2) by Eq. (6):

$$\mathbf{P}(\hat{\mathbf{k}}_1,\hat{\mathbf{k}}_2)=\frac{(1-g^2)}{2\pi(1+2g\cos\theta+g^2)^{3/2}}\frac{\mathbf{M}(\mathbf{J}_{\rm vol})}{(1+\cos^2\theta)}\,. \tag{7}$$

We should note here that there is some arbitrariness adopted in our derivation of Eq. (7). We could have foregone the normalization given in Eq. (6), which would have made the choice of g = 0 correspond to the Rayleigh scattering function. We chose instead to keep the meaning of the phase function as a description of a probability distribution. Since the Henyey-Greenstein function is only an empirical parameterization of the phase function, the choice here is one of personal taste.

2.2. Single volume scattering beneath a flat interface

We now develop a theory for reflective scattering of light by a volume diffuser beneath a smooth interface. There are two limits that we consider: the single scattering limit and the diffuse scattering limit. In the next section, we will consider the diffuse scattering limit. In the single scattering limit, discussed in this section, we only consider a single interaction with the volume diffuser. That is, rays are allowed to be incident upon the material, refract into the material, scatter once using the phase function given in Sec. 2.1, and refract out of the material. All rays which scatter more than once in the volume are ignored.

We begin by defining unit vectors which are convenient for describing the electric field for various rays. For any ray propagating in the direction of unit vector $\hat{\mathbf{k}}$, we define polarization vectors

$$\hat{\mathbf{s}}=\hat{\mathbf{k}}\times\hat{\mathbf{n}}/\left|\hat{\mathbf{k}}\times\hat{\mathbf{n}}\right| \text{ and } \hat{\mathbf{p}}=\hat{\mathbf{k}}\times\hat{\mathbf{s}}\,, \tag{8}$$

where $\hat{\mathbf{n}}$ is the surface normal, which in this section is the same as the unit vector in the z direction, $\hat{\mathbf{z}}$. An index is affixed to these vectors to indicate those associated with the incident direction (i) or the reflected (scattered) direction (r). A prime is affixed to these unit vectors if they represent propagation inside the material. That is, by Snell's law,

$$\hat{\mathbf{k}}\times\hat{\mathbf{n}}=n\hat{\mathbf{k}}'\times\hat{\mathbf{n}}\,, \tag{9}$$

where n is the index of refraction of the material. The dyadic relating the incident amplitude to the transmitted amplitude of the incident ray entering the material is given by

$$\ddot{\mathbf{t}}_{\rm i}=(t_{\rm is}\hat{\mathbf{s}}'_{\rm i}\hat{\mathbf{s}}_{\rm i}+t_{\rm ip}\hat{\mathbf{p}}'_{\rm i}\hat{\mathbf{p}}_{\rm i})\,, \tag{10}$$

where the amplitude transmission coefficients are $t_{\rm is}$ and $t_{\rm ip}$ evaluated at the incident direction for s and p polarized light, respectively. The equivalent dyadic for a ray transmitting out of the material is

$$\ddot{\mathbf{t}}_{\rm r}=\frac{n\cos\theta'_{\rm r}}{\cos\theta_{\rm r}}(t_{\rm rs}\hat{\mathbf{s}}_{\rm r}\hat{\mathbf{s}}'_{\rm r}+t_{\rm rp}\hat{\mathbf{p}}_{\rm r}\hat{\mathbf{p}}'_{\rm r})\,. \tag{11}$$

where the amplitude transmission coefficients, $t_{\rm rs}$ and $t_{\rm rp}$, are evaluated in the scattering direction for light incident from the air. The net scattering dyadic is thus given by combining Eqs. (4), (10), and (11):

$$\ddot{\mathbf{q}}_{\rm vol}=\frac{n\cos\theta'_{\rm r}}{\cos\theta_{\rm r}}(t_{\rm rs}\hat{\mathbf{s}}_{\rm r}\hat{\mathbf{s}}'_{\rm r}+t_{\rm rp}\hat{\mathbf{p}}_{\rm r}\hat{\mathbf{p}}'_{\rm r})\cdot(\hat{\boldsymbol{\sigma}}_2\hat{\boldsymbol{\sigma}}_2+\hat{\boldsymbol{\pi}}_2\hat{\boldsymbol{\pi}}_2)\cdot(t_{\rm is}\hat{\mathbf{s}}'_{\rm i}\hat{\mathbf{s}}_{\rm i}+t_{\rm ip}\hat{\mathbf{p}}'_{\rm i}\hat{\mathbf{p}}_{\rm i})\,. \tag{12}$$

The Jones matrix associated with Eq. (12) is

$$\mathbf{J}_{\rm vol}=\begin{pmatrix}\hat{\mathbf{s}}_{\rm r}\cdot\ddot{\mathbf{q}}_{\rm vol}\cdot\hat{\mathbf{s}}_{\rm i} & \hat{\mathbf{s}}_{\rm r}\cdot\ddot{\mathbf{q}}_{\rm vol}\cdot\hat{\mathbf{p}}_{\rm i}\\ \hat{\mathbf{p}}_{\rm r}\cdot\ddot{\mathbf{q}}_{\rm vol}\cdot\hat{\mathbf{s}}_{\rm i} & \hat{\mathbf{p}}_{\rm r}\cdot\ddot{\mathbf{q}}_{\rm vol}\cdot\hat{\mathbf{p}}_{\rm i}\end{pmatrix}=\frac{n\cos\theta'_{\rm r}}{\cos\theta_{\rm r}}\begin{pmatrix}q_{\rm ss}^{\rm vol} & q_{\rm ps}^{\rm vol}\\ q_{\rm sp}^{\rm vol} & q_{\rm pp}^{\rm vol}\end{pmatrix}, \tag{13}$$

where

$$q_{\rm ss}^{\rm vol}=t_{\rm is}t_{\rm rs}\cos\phi_{\rm r}\,,$$

$$q_{\mathrm{sp}}^{\mathrm{vol}} = -t_{\mathrm{is}} t_{\mathrm{rp}} \cos\theta_{\mathrm{r}}' \sin\phi_{\mathrm{r}} ,$$

$$q_{\mathrm{ps}}^{\mathrm{vol}} = t_{\mathrm{ip}} t_{\mathrm{rs}} \cos\theta_{\mathrm{i}}' \sin\phi_{\mathrm{r}} ,$$

$$q_{\mathrm{pp}}^{\mathrm{vol}} = t_{\mathrm{ip}} t_{\mathrm{rp}} (\cos\theta_{\mathrm{i}}' \cos\theta_{\mathrm{r}}' \cos\phi_{\mathrm{r}} + \sin\theta_{\mathrm{i}}' \sin\theta_{\mathrm{r}}') .$$

The Mueller matrix ray energy equivalent of Eq. (12) is

$$\frac{n\cos\theta_{\mathrm{i}}'}{\cos\theta_{\mathrm{i}}} \frac{\cos\theta_{\mathrm{r}}}{n\cos\theta_{\mathrm{r}}'} \mathbf{M}(\mathbf{J}_{\mathrm{vol}}) = \frac{n^2 \cos\theta_{\mathrm{i}}' \cos\theta_{\mathrm{r}}'}{\cos\theta_{\mathrm{i}} \cos\theta_{\mathrm{r}}} \mathbf{M} \begin{pmatrix} q_{\mathrm{ss}}^{\mathrm{vol}} & q_{\mathrm{ps}}^{\mathrm{vol}} \\ q_{\mathrm{sp}}^{\mathrm{vol}} & q_{\mathrm{pp}}^{\mathrm{vol}} \end{pmatrix}, \tag{14}$$

where we have included factors which account for the amplitude/ray energy relationship. The factor relating a solid angle inside the material $\mathrm{d}\Omega_{\mathrm{r}}'$ to that outside the material $\mathrm{d}\Omega_{\mathrm{r}}$ is given by

$$\frac{\mathrm{d}\Omega_{\mathrm{r}}'}{\mathrm{d}\Omega_{\mathrm{r}}} = \frac{\sin\theta_{\mathrm{r}}'}{\sin\theta_{\mathrm{r}}} \begin{vmatrix} \partial\theta_{\mathrm{r}}'/\partial\theta_{\mathrm{r}} & \partial\phi_{\mathrm{r}}'/\partial\theta_{\mathrm{r}} \\ \partial\theta_{\mathrm{r}}'/\partial\phi_{\mathrm{r}} & \partial\phi_{\mathrm{r}}'/\partial\phi_{\mathrm{r}} \end{vmatrix} = \frac{\cos\theta_{\mathrm{r}}}{n^2\cos\theta_{\mathrm{r}}'} . \tag{15}$$

Suppose that the material has a scattering mean free path *l*. Then the probability that a ray will scatter at a distance between ξ and $\xi + \mathrm{d}\xi$ in the material will be

$$p_1(\xi)\,\mathrm{d}\xi = \frac{1}{l}\exp(-\xi/l)\,\mathrm{d}\xi . \tag{16}$$

The probability that the ray will travel a distance at least ξ is given by

$$p_2(\xi) = \int_{\xi}^{\infty} p_1(\xi')\mathrm{d}\xi' = \exp(-\xi/l) . \tag{17}$$

Therefore, the probability that a ray incident inside the material at an angle θ_{i}' scatters at a depth *z* into an angle θ_{r}', and makes it back to the surface is given by

$$p_3(z)\,\mathrm{dz} = p_1(z)\,p_2(z)\,\mathrm{dz} = \frac{1}{l\cos\theta_{\mathrm{i}}'}\exp[-z/(l\cos\theta_{\mathrm{i}}')]\exp[-z/(l\cos\theta_{\mathrm{r}}')]\,\mathrm{dz} . \tag{18}$$

If we consider all scattering depths, the probability of a ray scattering once and returning to the surface is given by

$$p_4 = \int_0^{\infty} p_3(z)\,\mathrm{dz} = \frac{\cos\theta_{\mathrm{r}}'}{\cos\theta_{\mathrm{i}}' + \cos\theta_{\mathrm{r}}'} . \tag{19}$$

The net Mueller matrix BRDF is found by combining Eqs. (1), (6), (14), (15), and (19):

$$\begin{aligned} \mathbf{f}_{\mathrm{vol}} &= p(\theta)\frac{p_4}{\cos\theta_{\mathrm{r}}} \mathbf{M} \begin{pmatrix} q_{\mathrm{ss}}^{\mathrm{vol}} & q_{\mathrm{ps}}^{\mathrm{vol}} \\ q_{\mathrm{sp}}^{\mathrm{vol}} & q_{\mathrm{pp}}^{\mathrm{vol}} \end{pmatrix} \frac{d\Omega_{\mathrm{r}}}{d\Omega_{\mathrm{r}}'} \frac{2}{(1+\cos^2\theta)} \frac{n^2\cos\theta_{\mathrm{i}}'\cos\theta_{\mathrm{r}}'}{\cos\theta_{\mathrm{i}}\cos\theta_{\mathrm{r}}} \\ &= \frac{2\,p(\theta)\cos\theta_{\mathrm{i}}'\cos\theta_{\mathrm{r}}'}{\cos\theta_{\mathrm{i}}\cos\theta_{\mathrm{r}}(\cos\theta_{\mathrm{i}}' + \cos\theta_{\mathrm{r}}')(1+\cos^2\theta)} \mathbf{M} \begin{pmatrix} q_{\mathrm{ss}}^{\mathrm{vol}} & q_{\mathrm{ps}}^{\mathrm{vol}} \\ q_{\mathrm{sp}}^{\mathrm{vol}} & q_{\mathrm{pp}}^{\mathrm{vol}} \end{pmatrix}. \end{aligned} \tag{20}$$

An implementation of the theory described in this section can be found in the SCATMECH library[18] of scattering codes, as FIRST_DIFFUSE_BRDF_MODEL.

2.3. Totally diffuse scattering beneath a flat interface

In the limit of completely diffusive scatter, we assume that the BRDF of the underlying material is totally depolarizing and is a constant given by ρ/π, where ρ is the reflectance of the material. The Mueller matrix probability of an incident ray scattering into a direction θ_{r}' and into solid angle $\mathrm{d}\Omega_{\mathrm{r}}'$ is then given by

$$\mathbf{D}(\rho/\pi)\cos\theta_r' \, d\Omega_r' \tag{21}$$

where $\mathbf{D}$ is the unit depolarizing Mueller matrix. The fraction of the diffusely scattered light which is reflected by the exposed interface is the weighted average reflectance of the top surface:

$$\bar{R} = \frac{1}{2\pi}\int \frac{1}{2}\left[\left|r_p(\theta_r')\right|^2 + \left|r_s(\theta_r')\right|^2 \right] \cos\theta_r' \, d\Omega_r' \, . \tag{22}$$

where $r_j(\theta_r')$ (j = s, p) is the internal reflection coefficient. The total intensity incident upon the diffuse material is that incident upon it directly, plus that which is diffusely reflected by the material but reflected back into it by the exposed interface. Therefore, the amount of light incident upon the material relative to that directly incident upon it is given by

$$1 + \rho\bar{R} + (\rho\bar{R})^2 + (\rho\bar{R})^3 + \cdots = \frac{1}{1-\rho\bar{R}} \, . \tag{23}$$

The Mueller matrix transmittance for light transmitting into the material is given by

$$\frac{n\cos\theta_i'}{\cos\theta_i}\mathbf{M}\begin{pmatrix} t_{is} & 0 \\ 0 & t_{ip} \end{pmatrix}. \tag{24}$$

The Mueller matrix transmittance for light exiting through the exposed interface is given by

$$\frac{n\cos\theta_r'}{\cos\theta_r}\mathbf{M}\begin{pmatrix} t_{rs} & 0 \\ 0 & t_{rp} \end{pmatrix}. \tag{25}$$

In Eq. (25), we have made use of the reciprocity of the transmittance. As in Sec. 2.2, the transmission coefficients in Eqs. (24) and (25) are those for light incident from the air, evaluated at the incident and reflected directions, respectively. The net Mueller matrix probability for an incident ray scattering into direction θ_r about solid angle $d\Omega_r$ is found by combining Eqs. (21), (23), (24), and (25):

$$\begin{aligned} \mathbf{P}_{diff} &= \frac{n\cos\theta_r'}{\cos\theta_r}\mathbf{M}\begin{pmatrix} t_{rs} & 0 \\ 0 & t_{rp} \end{pmatrix}\mathbf{D}(\rho/\pi)\frac{1}{1-\rho R}\cos\theta_r'\frac{n\cos\theta_i'}{\cos\theta_i}\mathbf{M}\begin{pmatrix} t_{is} & 0 \\ 0 & t_{ip} \end{pmatrix} d\Omega_r' \\ &= \mathbf{M}\begin{pmatrix} t_{rs} & 0 \\ 0 & t_{rp} \end{pmatrix}\mathbf{D}\mathbf{M}\begin{pmatrix} t_{is} & 0 \\ 0 & t_{ip} \end{pmatrix}\frac{(\rho/\pi)}{1-\rho R}\cos\theta_r'\frac{\cos\theta_i'}{\cos\theta_i} d\Omega_r \end{aligned} \, . \tag{26}$$

That is, the Mueller matrix BRDF is given by

$$\mathbf{f}_{diff} = \mathbf{M}_{diff}\frac{(\rho/\pi)}{(1-\rho\bar{R})}\frac{\cos\theta_r'\cos\theta_i'}{\cos\theta_r\cos\theta_i} \, . \tag{27}$$

where the matrix $\mathbf{M}_{diff}$ has four non-zero elements:

$$\begin{aligned} M_{diff,00} &= (|t_{rs}|^2 + |t_{rp}|^2)(|t_{is}|^2 + |t_{ip}|^2)/4 \\ M_{diff,01} &= (|t_{rs}|^2 + |t_{rp}|^2)(|t_{is}|^2 - |t_{ip}|^2)/4 \\ M_{diff,10} &= (|t_{rs}|^2 - |t_{rp}|^2)(|t_{is}|^2 + |t_{ip}|^2)/4 \\ M_{diff,11} &= (|t_{rs}|^2 - |t_{rp}|^2)(|t_{is}|^2 - |t_{ip}|^2)/4 \end{aligned} \tag{28}$$

We have verified that for an infinite, non-absorbing substrate, i.e., for $\rho = 1$, that the system has unit total integrated reflectance. An implementation of the theory described in this section can be found in the SCATMECH library[18] of scattering codes, as DIFFUSE_SUBSURFACE_BRDF_MODEL.

2.4. Rough surface scattering in transmission

Reflection scattering by a rough surface in the facet approximation is well known and discussed in depth in the literature.[13,19,20] There exists, however, very little discussion on facet scattering in transmission, and that which exists lacks theoretical basis.[21] In this section, we develop a theory for transmissive scattering by a rough surface using the facet approximation. We begin by assuming that the rough surface is isotropically rough and can be treated as a locally flat surface, with a local surface normal given in spherical coordinates by a polar angle θ_{n} and azimuthal angle ϕ_{n}. The local slope is given in the *x* and *y* directions by $\zeta_x = \tan\theta_{\mathrm{n}}\cos\phi_{\mathrm{n}}$ and $\zeta_y = \tan\theta_{\mathrm{n}}\sin\phi_{\mathrm{n}}$, respectively. The surface statistics can be described by a slope distribution function $P(\zeta)$, where $\zeta = \sqrt{\zeta_x^{\,2} + \zeta_y^{\,2}}$. This function is defined such that the probability of ζ_x being between ζ_x and $\zeta_x + \mathrm{d}\zeta_x$, and ζ_y being between ζ_y and $\zeta_y + \mathrm{d}\zeta_y$, choosing a point uniformly on the mean surface plane, is

$$P(\zeta)\,\mathrm{d}\zeta_x\mathrm{d}\zeta_y\,. \tag{29}$$

A ray which is incident upon this rough surface with a direction given by unit vector $\hat{\mathbf{k}}_{\mathrm{i}}$ and which transmits into a direction given by unit vector $\hat{\mathbf{k}}_{\mathrm{t}}$ is assumed to have struck a single interface oriented with a unit surface normal $\hat{\mathbf{n}}$, such that the rays are related by the Snell's law:

$$\hat{\mathbf{k}}_{\mathrm{i}} \times \hat{\mathbf{n}} = n\,\hat{\mathbf{k}}_{\mathrm{t}} \times \hat{\mathbf{n}}\,. \tag{30}$$

where *n* is the index of refraction of the substrate material. Given $\hat{\mathbf{k}}_{\mathrm{i}}$, $\hat{\mathbf{k}}_{\mathrm{t}}$, and *n*, we find that

$$\hat{\mathbf{n}} = \pm\hat{\mathbf{x}}(\sin\theta_{\mathrm{i}} - n\cos\phi_{\mathrm{t}}\sin\theta_{\mathrm{t}})/D \mp \hat{\mathbf{y}}n\sin\phi_{\mathrm{t}}\sin\theta_{\mathrm{t}}/D \pm \hat{\mathbf{z}}(n\cos\theta_{\mathrm{t}} - \cos\theta_{\mathrm{i}})/D \tag{31}$$

are solutions to Eq. (30), where

$$D = \sqrt{1 - 2n\cos\theta_{\mathrm{i}}\cos\theta_{\mathrm{t}} - 2n\sin\theta_{\mathrm{i}}\sin\theta_{\mathrm{t}}\cos\phi_{\mathrm{t}} + n^2}\,. \tag{32}$$

We choose the signs in Eq. (31) so that the *z* component of $\hat{\mathbf{n}}$ is positive. The local angle of incidence onto the facet is

$$\iota_{\mathrm{i}} = \arccos(\hat{\mathbf{k}}_{\mathrm{i}} \cdot \hat{\mathbf{n}})\,, \tag{33}$$

and the local angle of transmittance is

$$\iota_{\mathrm{t}} = \arccos(\hat{\mathbf{k}}_{\mathrm{t}} \cdot \hat{\mathbf{n}})\,. \tag{34}$$

The slope of this facet is

$$\zeta = [(n_x/n_z)^2 + (n_y/n_z)^2]^{1/2}\,. \tag{35}$$

The angles given in Eqs. (33) and (34) must lie between 0 and π/2 in order for the analysis to be valid. That is, there are combinations of incident and transmitted directions for which no facet can exist with positive slope that refracts one into the other.

The probability given in Eq. (29) is for points sampled uniformly on the *xy* plane. If one considers the slope distribution for points sampled uniformly on a plane perpendicular to the incident direction, that is, the probability for striking a facet of a specific slope, then one has

$$P'(\zeta) \propto P(\zeta)\cos\iota_{\mathrm{i}}\sec\theta_{\mathrm{n}}\,. \tag{36}$$

To normalize this distribution function, we assume that the slope distribution is sufficiently narrow that $\langle\cos\iota_{\mathrm{i}}\rangle \cong \cos\theta_{\mathrm{i}}$. Then

$$P'(\zeta) \cong P(\zeta)\cos\iota_{\mathrm{i}}\sec\theta_{\mathrm{i}}\sec\theta_{\mathrm{n}}\,. \tag{37}$$

The probability distribution $P'(\zeta)$ is the probability per unit differential slope $\mathrm{d}\zeta_x \mathrm{d}\zeta_y$ that a ray will scatter into a direction $\hat{\mathbf{k}}_\mathrm{t}$. We are interested, however, in the probability per unit solid angle $\mathrm{d}\Omega_\mathrm{t} = \sin\theta_\mathrm{t}\mathrm{d}\theta_\mathrm{t}\mathrm{d}\phi_\mathrm{t}$. We make the necessary change of variables in two steps. First, we change from slope coordinates to solid angle subtended by the surface normal using the factor

$$\frac{\mathrm{d}\zeta_x \mathrm{d}\zeta_y}{\mathrm{d}\Omega_\mathrm{n}} = \frac{1}{\sin\theta_\mathrm{n}} \begin{vmatrix} \partial\zeta_x/\partial\theta_\mathrm{n} & \partial\zeta_x/\partial\phi_\mathrm{n} \\ \partial\zeta_y/\partial\theta_\mathrm{n} & \partial\zeta_y/\partial\phi_\mathrm{n} \end{vmatrix} = \sec^3\theta_\mathrm{n} . \tag{38}$$

Next, the ratio of the differential solid angles subtended by the surface normal $\mathrm{d}\Omega_\mathrm{n}$ to that subtended by the scattering direction, $\mathrm{d}\Omega_\mathrm{t}$, is found to be

$$\begin{aligned} \frac{\mathrm{d}\Omega_\mathrm{n}}{\mathrm{d}\Omega_\mathrm{t}} &= \frac{\sin\theta_\mathrm{n}}{\sin\theta_\mathrm{t}} \begin{vmatrix} \partial\theta_\mathrm{n}/\partial\theta_\mathrm{t} & \partial\phi_\mathrm{n}/\partial\theta_\mathrm{t} \\ \partial\theta_\mathrm{n}/\partial\phi_\mathrm{t} & \partial\phi_\mathrm{n}/\partial\phi_\mathrm{t} \end{vmatrix} \\ &= (n^2\{-[n(3+\cos 2\theta_\mathrm{t})\cos\theta_\mathrm{i}] + \cos\phi_\mathrm{t}\sin 2\theta_\mathrm{i}\sin\theta_\mathrm{t} + \cos\theta_\mathrm{t}\cos^2\theta_\mathrm{i} + \\ &\qquad \cos\theta_\mathrm{t}(1 - 2n\cos\phi_\mathrm{t}\sin\theta_\mathrm{i}\sin\theta_\mathrm{t} + 2n^2 - \sin^2\theta_\mathrm{i})\})/[2D^3(\, n\cos\theta_\mathrm{t} - \cos\theta_\mathrm{i})] \end{aligned} \tag{39}$$

We let the transmission coefficients for light incident onto the surface at an angle ι_i be t_s and t_p for s- and p-polarized light, respectively. The transmission dyadic is given by

$$\ddot{\mathbf{t}}_\mathrm{facet} = (\hat{\mathbf{s}}_\mathrm{t}\hat{\mathbf{s}}'_\mathrm{t} + \hat{\mathbf{p}}_\mathrm{t}\hat{\mathbf{p}}'_\mathrm{t}) \cdot (\hat{\mathbf{s}}'_\mathrm{t}\hat{\mathbf{s}}'_\mathrm{i} t_\mathrm{s} + \hat{\mathbf{p}}'_\mathrm{t}\hat{\mathbf{p}}'_\mathrm{i} t_\mathrm{p}) \cdot (\hat{\mathbf{s}}'_\mathrm{i}\hat{\mathbf{s}}_\mathrm{i} + \hat{\mathbf{p}}'_\mathrm{i}\hat{\mathbf{p}}_\mathrm{i}) , \tag{40}$$

where

$$\hat{\mathbf{s}}_j = \hat{\mathbf{k}}_j \times \hat{\mathbf{z}} / \left|\hat{\mathbf{k}}_j \times \hat{\mathbf{z}}\right| , \quad \hat{\mathbf{p}}_j = \hat{\mathbf{k}}_j \times \hat{\mathbf{s}}_j$$

$$\hat{\mathbf{s}}'_j = \hat{\mathbf{k}}_j \times \hat{\mathbf{n}} / \left|\hat{\mathbf{k}}_j \times \hat{\mathbf{n}}\right| , \quad \hat{\mathbf{p}}'_j = \hat{\mathbf{k}}_j \times \hat{\mathbf{s}}'_j$$

(j = i, t) are unit polarization vectors in the global and local coordinates, respectively. After a considerable amount of algebra, we find the Jones matrix associated with the dyadic $\ddot{\mathbf{t}}_\mathrm{facet}$:

$$\mathbf{J}_\mathrm{facet} = \frac{1}{\sqrt{F_1 F_2}} \begin{pmatrix} (t_\mathrm{p}a_2 + t_\mathrm{s}a_1) & (t_\mathrm{p}a_4 - t_\mathrm{s}a_3) \\ (t_\mathrm{p}a_3 - t_\mathrm{s}a_4) & (t_\mathrm{p}a_1 + t_\mathrm{s}a_2) \end{pmatrix} \tag{41}$$

where

$$\begin{aligned} a_1 &= (\cos\theta_\mathrm{n}\sin\theta_\mathrm{i} + \cos\phi_\mathrm{n}\cos\theta_\mathrm{i}\cos\theta_\mathrm{n})\cos\theta_\mathrm{t}\sin\theta_\mathrm{n}\cos(\phi_\mathrm{n} - \phi_\mathrm{t}) + \\ &\qquad (\cos\theta_\mathrm{n}\sin\theta_\mathrm{i} + \cos\phi_\mathrm{n}\cos\theta_\mathrm{i}\sin\theta_\mathrm{n})\cos\theta_\mathrm{n}\sin\theta_\mathrm{t} \end{aligned}$$

$$a_2 = \sin\phi_\mathrm{n}\sin(\phi_\mathrm{n} - \phi_\mathrm{t})\sin^2\theta_\mathrm{n}$$

$$a_3 = [\cos\theta_\mathrm{n}\sin\phi_\mathrm{n}\sin\theta_\mathrm{t} + \cos\theta_\mathrm{t}\sin\phi_\mathrm{n}\sin\theta_\mathrm{n}\cos(\phi_\mathrm{n} - \phi_\mathrm{t})]\sin\theta_\mathrm{n}$$

$$a_4 = (\cos\theta_\mathrm{n}\sin\theta_\mathrm{i} + \cos\phi_\mathrm{n}\cos\theta_\mathrm{i}\sin\theta_\mathrm{n})\sin\theta_\mathrm{n}\sin(\phi_\mathrm{n} - \phi_\mathrm{t})$$

$$F_1 = 2\cos\phi_\mathrm{n}\cos\theta_\mathrm{i}\cos\theta_\mathrm{n}\sin\theta_\mathrm{i}\sin\theta_\mathrm{n} + \cos^2\theta_\mathrm{n}\sin^2\theta_\mathrm{i} + (\cos^2\phi_\mathrm{n}\cos^2\theta_\mathrm{i} + \sin^2\phi_\mathrm{n})\sin^2\theta_\mathrm{n}$$

$$F_2 = \sin^2\theta_\mathrm{n}\sin^2\theta_\mathrm{t}\sin^2(\phi_\mathrm{n} - \phi_\mathrm{t}) + (\cos\phi_\mathrm{n}\cos\theta_\mathrm{t}\sin\theta_\mathrm{n} + \cos\phi_\mathrm{t}\cos\theta_\mathrm{n}\sin\theta_\mathrm{t})^2 + (\cos\theta_\mathrm{t}\sin\phi_\mathrm{n}\sin\theta_\mathrm{n} + \cos\theta_\mathrm{n}\sin\phi_\mathrm{t}\sin\theta_\mathrm{t})^2$$

The Mueller matrix transmittance is

$$\mathbf{M}_\mathrm{facet} = \frac{n\cos\iota_\mathrm{t}}{\cos\iota_\mathrm{i}} \mathbf{M}(\mathbf{J}_\mathrm{facet}) \tag{42}$$

The Mueller matrix BTDF is thus found by combining Eqs. (1), (37), (38), (39), and (42):

$$\mathbf{f}_{\text{facet}} = \frac{\mathrm{d}\Omega_{\text{n}}}{\mathrm{d}\Omega_{\text{t}}} \frac{n \cos \iota_{\text{t}} \sec^4 \theta_{\text{n}}}{\cos \theta_{\text{i}} \cos \theta_{\text{t}}} P(\zeta) \mathbf{M}(\mathbf{J}_{\text{facet}}) \tag{43}$$

An implementation of the theory described in this section can be found in the SCATMECH library[18] of scattering codes, as FACET_BRDF_MODEL.

2.5. Single and diffusive volume scattering beneath a rough surface

Reflective scattering by a diffuse substrate beneath a rough surface requires combining the models described in the sections above. Any ray which scatters in the diffuse substrate and is re-reflected must necessarily undergo at least three scattering events, two at the rough surface and one in the bulk. For that reason, there must be an appropriate averaging over the propagation directions in the bulk. This averaging can be performed in a variety of ways. Here, we chose to perform the averaging by a Monte Carlo method, which we outline below.

We begin by choosing a slope distribution function, and creating a random surface normal generator that reproduces the particular distribution when sampled uniformly on the *xy* plane. Due to the assumed isotropy of the surface, such a distribution is uniform in azimuthal angle ϕ_{n}, and so one only needs to select angles θ_{n}. We must create a second random surface normal generator which reproduces the distribution sampled uniformly by the incident rays propagating at an oblique angle. For oblique incidence, this second distribution will not be uniform in ϕ_{n}. If our external propagation direction is $\hat{\mathbf{k}}$ (and this can be an incident or a scattered direction), we choose a surface normal $\hat{\mathbf{n}}$ from the distribution using the first random surface normal generator. We then determine the projection of the incident direction onto that surface normal, $\hat{\mathbf{k}} \cdot \hat{\mathbf{n}}$, and, if the projection is positive, we choose a uniform random number in the range (0,1). We continue to choose surface normals until the uniform random number is less than the projection. The resulting surface normal will reproduces the distribution sampled uniformly by the incident rays.

We assume that the scattering occurs deep enough into the material that the facet that a ray enters the material is different than the facet the ray exits. For a given incident and scattering direction, we choose two surface normals, one for the incident direction and one for the scattering direction. By Snell's law [Eq. (30)], these each uniquely determine the directions of propagation inside the material, and the Mueller matrix transmittance through the facets. We then apply the scattering functions given by Eqs. (7) and (21) to determine the probability for single and multiple scattering into this direction. We average the resulting scattering probability over an ensemble of pairs of surface normals. Generally, about 50 pairs of surface normals are required to obtain sufficient statistics to match that of the data, and about 5000 pairs of surface normals to obtain a smooth curve. We also calculate the direct reflective scattering from the rough surface in the facet approximation, using the slope distribution function.[13,19,20] This contribution is added to the total calculated scatter.

3. EXPERIMENT

Measurements were performed using the Goniometric Optical Scatter Instrument (GOSI) at NIST.[22,23] GOSI is a laser-based angle-resolved scattering system having a high angular resolution, wide dynamic range, full polarimetric capabilities, and the ability to measure scattering in and out of the plane of incidence. Measurements were performed using a fixed incident angle (θ_{i} = 60°), scanning the scattering angle in the plane of incidence and using either a HeNe laser (λ = 632.8 nm) or a HeCd laser (λ = 441.6 nm). While the instrument is capable of full Mueller matrix measurements, only measurements of the Stokes vector were performed, using 45° incident polarization, a configuration which yields a high degree of discrimination between scattering sources. For measurements carried out at 441.6 nm, an interference bandpass filter was used to remove most of the sample fluorescence from the signal.

The intensity and polarization of the scattered light is characterized by the polarization-averaged bidirectional reflectance distribution function (BRDF), f_{r}, the principal angle of the polarization, η (measured counterclockwise from s-polarization when looking into the direction of propagation), the degree of circular polarization, P_{C}, and the total degree of polarization, P. These parameters can be obtained from the Stokes parameters. While use of the linear Stokes parameters simplifies many calculations, presentation of data with the parameters η, P_{C}, and P often simplifies

interpretation. In particular, η and P_C parameterize the polarization state of the polarized part of the beam, while P characterizes the unpolarized part. Furthermore, for many scattering mechanisms and experimental geometries, P_C is close to zero, so that η alone distinguishes amongst dominant scattering mechanisms.

All of the measurements were performed on nine different spots on the sample. The statistical sources of error are believed to dominate the uncertainty in these measurements. Therefore, all experimental data are shown as marks whose length represent the standard deviation of the mean of the measurements or 68 % confidence levels.

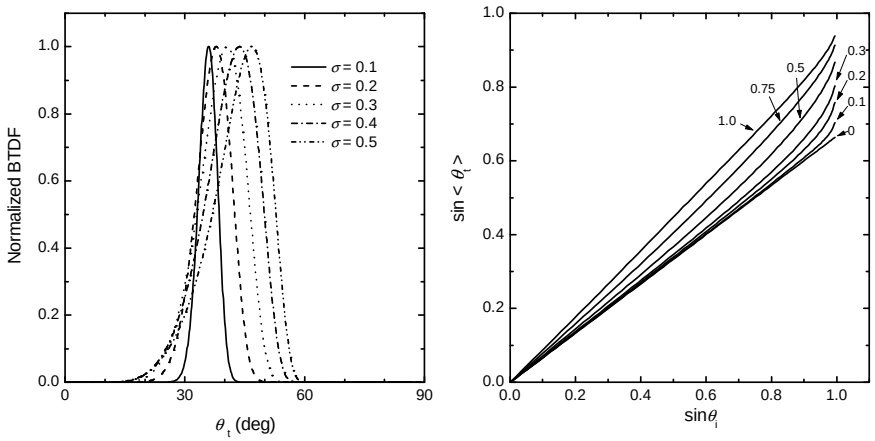

Figure 1. (left) The BTDF, normalized to its peak value, for a variety of Gaussian slope distribution functions, calculated using the facet scattering model in transmission. The standard deviation of the slope, σ, is indicated in the figure. The incident angle was 60° and the index of refraction was 1.5. (right) The sine of the BTDF-weighted-mean of the scattering angle as a function of the sine of the incident angle for the facet scattering model in transmission.

4. RESULTS AND DISCUSSION

Figure 1(left) shows calculated BTDFs, normalized by their peak values, for scattering in transmission for a variety of slope distribution functions. The material was assumed to have an index of refraction of n = 1.5, and the incident angle for the calculations was $\theta_i = 60°$, which corresponds to a normally refracted angle of $\theta_t = 35.3°$. The facet distribution functions were all Gaussian in slope, with different slope standard deviations σ. For the narrowest slope distribution, the angle at which the BTDF peaks occurs is at $\theta_t = 36°$, close to the normal refraction angle. As the slope distribution widens, the BTDF widens and the peak shifts to larger angle, eventually approaching nearly the same angle as the incident angle. This behavior is characteristic of scattering by surface facets in transmission. As the distribution gets wider, those facets which present themselves most strongly to the incident beam dominate the distribution as observed by the incident beam, and these facets refract the angle the least. In Fig. 1(right), we show the calculated sine of the mean refraction angle as a function of the sine of the incident angle, for different σ. For narrow slope distributions, the results show a linear relationship with slope 1/n, as expected from Snell's law. As the distribution is widened, the results indicate that the mean scattering angle follows Snell's law approximately, but with a substantially lower index of refraction.

Figure 2(left) shows measurement results for the scattering by a glossy white paint, measured using λ = 632.8 nm, along with calculated results for totally diffuse scattering beneath a smooth interface (solid curve). The index of refraction n was approximately 1.5 and the substrate diffuse reflectance ρ was set to 0.93 to obtain good results. The theory predicts the principal angle of the polarization η to be ±90°. In the near specular direction, the scattering is dominated by the roughness of the exposed interface, and the polarization in this region confirms this interpretation (dashed curve). In the rest of the measured range, the calculated BRDF and the polarization state matches the measurements very well. The shape of the BRDF, for example, shows a large flat region curving downward at large angles, which results from the angle dependence of the transmission coefficients. The scattered light is highly depolarized, except at large angles, where the difference between transmission of s- and p-polarized light results in an

excess of p-polarized light and a rise in the degree of polarization. There is also no measurable degree of circular polarization. For most of the measured range, the direction of the polarization is poorly defined, due to the low degree of polarization.

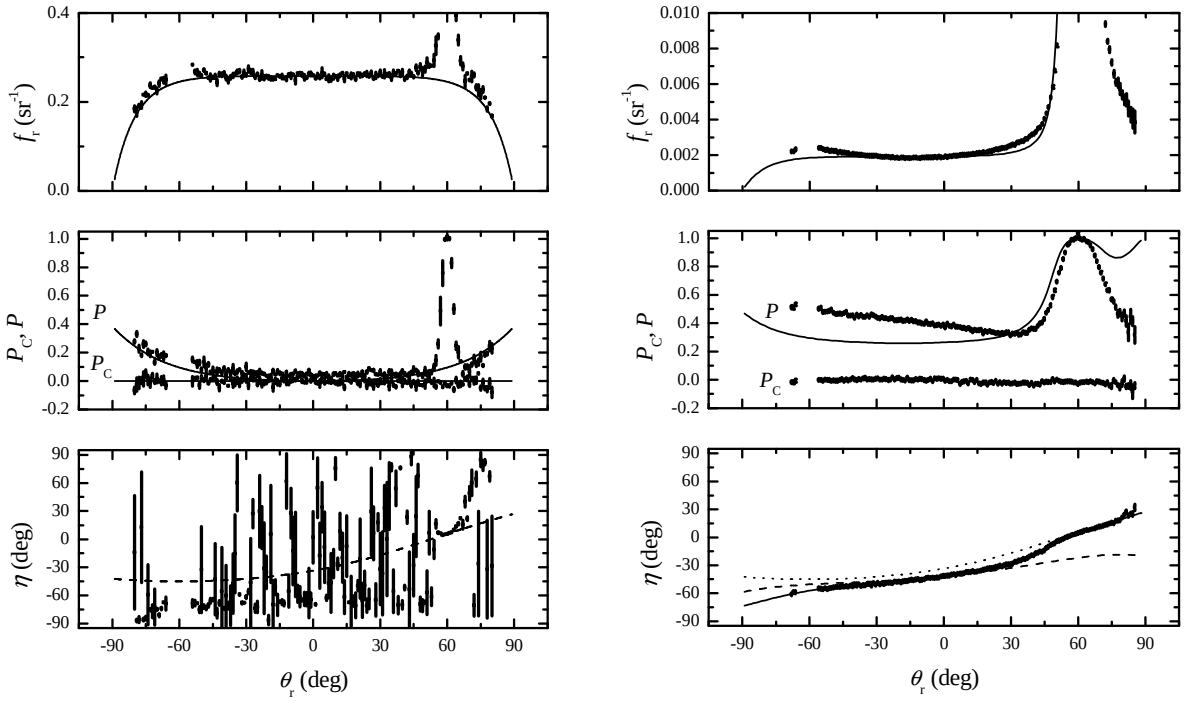

Figure 2. (left) Light scattering parameters for a glossy white paint measured at λ = 632.8 nm. The model curves represent the subsurface diffuse scattering model (solid) and the facet scattering model (dashed) as described in the text. (right). Light scattering parameters for a glossy red pigmented paint measured at λ = 441.6 nm. The model curves represent the facet scattering model (dotted), the single volume scattering model (dashed), and the combination model (solid) as described in the text.

Figure 2(right) shows measurement results for a red pigmented paint coating, measured at λ = 442 nm, where the reflectance of the material is relatively low. In this sample, it is expected that the signal will be dominated at large angles by single volume scattering in the pigmented layer. Fig. 2(right) shows three theoretical curves for the parameter η. The dotted curve corresponds to that predicted by the reflective facet scattering model and agrees well with the experimental data for a region near the specular direction. The dashed curve corresponds to that predicted by the single volume scattering model under a smooth surface, which agrees fairly well with the experimental data for angles farther from the specular direction. The agreement at very large angles is not perfect, however. A third theoretical curve was hand-fitted with an incoherent combination of the reflective facet scattering model, the single volume scattering model, and the totally diffuse volume scattering model. The agreement between the combination model and the experimental data is very good. The results for the combination model are also shown for P and the BRDF, and reasonable qualitative agreement is observed. The combination model is very similar to the model developed by Maxwell-Beard,[4] but differs in a number of features. The Maxwell-Beard model does not fully describe the polarization state, does not include material refraction, and accounts for the multiply diffuse scatter with only a Lambertian term, without including the interface as described in Sec. 2.3. The Maxwell-Beard model, however, includes a geometrical shadowing and obscuration factor, which we have chosen to ignore here.

Figure 3 shows measurement results for scattering by a green chemical agent resistant coating (CARC). This coating is very rough and exhibits no specular reflection peak. Data taken from a similar sample was interpreted in the past using a facet scattering model. However, as mentioned in the Introduction, it is difficult to reconcile the color (spectral dependence) of the scatter with any dependence on the dielectric function of the material. The solid curve passing through the data represents a calculation of the scattering by a diffuse material under a rough interface, as described in Sec. 2.5. The index of the binder material was assumed to be 1.5. The facet distribution was set to be

exponential in slope with a rms slope of 2, the Henyey-Greenstein *g*-factor was set to be 0.3, and the subsurface diffuse reflectance ρ was set to be 0.05. Despite the large rms slope, no shadowing was included in the calculation. There was no attempt to optimize these parameters, so they do not necessarily represent best fit parameters. The match of the parameter η to the measured values is very good. This is particularly significant, since this parameter was used previously to justify the use of the reflective facet scattering model for a similar sample, albeit with an unrealistic index of refraction.[13] The dashed curve represents the results of the reflective facet scattering model, using $n = 1.5$. While a very good agreement can be obtained using $n = 1.2$, such an index of refraction is unreasonable. For the CARC sample, we find reasonable agreement between the Monte Carlo model and the measured data without resorting to an unrealistic index. While other aspects of the calculation are not a perfect fit to the measured data, it can be considered to be surprisingly close considering the simplicity of the model and the lack of treatment of effects such as shadowing, retroreflection, and diffraction. While the model does not predict any circular polarization, the addition of the effect of absorbing pigments to the model would be expected to remedy that deficiency.

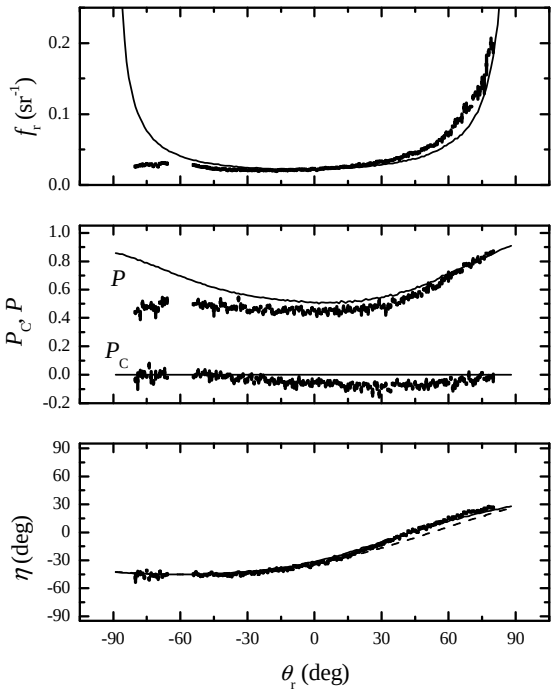

Figure 3. Light scattering parameters for a green chemical agent resistant coating (CARC) measured at $\lambda = 632.8$ nm. The model curves represent the predictions of the reflective facet scattering model (dashed) and the Monte Carlo model described in the text (solid).

The Maxwell-Beard model has been used with quite a bit of success to model the scattering by diffuse scattering paints.[4] Even if the model is extended to account for the polarization behavior of the facet and volume scattering terms, it does not account for refraction into and out of the material. For very rough surfaces, however, we found above that refraction from a rough surface tends to occur at a smaller angle than that predicted by the Snell's law, and seems to follow an approximate Snell's law behavior with a significantly lower index of refraction. This finding might explain the apparent success of the Maxwell-Beard model for very rough surfaces. Very rough surfaces enable one to ignore refraction in the material. What we hope to have developed here is an improvement on the Maxwell-Beard model that extends the range of materials that can be modeled.

ACKNOWLEDGEMENTS

The author would like to thank Dr. Maria Nadal of NIST for useful discussions and for providing samples and Dr. Mark Pesses of SAIC for providing samples.

REFERENCES

1. J.C. Stover, *Optical Scattering: Measurement and Analysis*, (SPIE Optical Engineering Press, Bellingham, WA, 1995).
2. T.A. Germer, G.W. Mulholland, J.H. Kim, and S.H. Ehrman, "Measurement of the 100 nm NIST SRM® 1963 by laser surface light scattering," in *Advanced Characterization Techniques for Optical, Semiconductor, and Data Storage Components*, A.Duparré and B.Singh, Eds., Proc. SPIE **4779**, 60-71, (2002)
3. J.C. Stover and C.A. Scheer, "Accurate sizing of deposited PSL spheres from light scatter measurements," in *Optical Metrology Roadmap for the Semiconductor, Optical, and Data Storage Industries II*, A. Duparré and B. Singh, Eds., Proc. SPIE **4449**, 147-150, (2001)
4. J.R. Maxwell, J. Beard, S. Weiner, D. Ladd, and D. Ladd, *Bidirectional Reflectance Model Validation and Utilization*, [Environmental Research Inst. of Michigan (ERIM), Ann Arbor, MI, 1973].
5. T.A. Germer and M.E. Nadal, "Modeling the appearance of special effect pigment coatings," in *Surface Scattering and Diffraction for Advanced Metrology*, Z.-H. Gu and A.A. Maradudin, Eds., Proc. SPIE **4447**, 77-86, (2001)
6. T.A. Germer, "Angular dependence and polarization of out-of-plane optical scattering from particulate contamination, subsurface defects, and surface microroughness," Appl. Opt. **36**, 8798-8805 (1997).
7. T.A. Germer, C.C. Asmail, and B.W. Scheer, "Polarization of out-of-plane scattering from microrough silicon," Opt. Lett. **22**, 1284-1286 (1997).
8. T.A. Germer and C.C. Asmail, "Polarization of light scattered by microrough surfaces and subsurface defects," J. Opt. Soc. Am. A **16**, 1326-1332 (1999).
9. T.A. Germer, "Measurement of roughness of two interfaces of a dielectric film by scattering ellipsometry," Phys. Rev. Lett. **85**, 349-352 (2000).
10. T.A. Germer, "Polarized light scattering by microroughness and small defects in dielectric layers," J. Opt. Soc. Am. A **18**, 1279-1288 (2001).
11. J.H. Kim, S.H. Ehrman, G.W. Mulholland, and T.A. Germer, "Polarized light scattering by dielectric and metallic spheres on silicon wafers," Appl. Opt. **41**, 5405-5412 (2002).
12. L. Sung, G.W. Mulholland, and T.A. Germer, "Polarized light-scattering measurements of dielectric spheres upon a silicon surface," Opt. Lett. **24**, 866-868 (1999).
13. R.G. Priest and T.A. Germer, "Polarimetric BRDF in the Microfacet Model: Theory and Measurements," in *Military Sensing Symposia (MSS) Specialty Group Meeting on Passive Sensors*, (Infrared Information Analysis Center, Ann Arbor, MI, 2000).
14. D.S. Flynn and C. Alexander, "Polarized surface scattering expressed in terms of a bidirectional reflectance distribution function matrix," Opt. Eng. **34**, 1646-1650 (1995).
15. F.E. Nicodemus, J.C. Richmond, J.J. Hsia, I.W. Ginsberg, and T. Limperis, *Geometrical Considerations and Nomenclature for Reflectance*, (National Bureau of Standards, Gaithersburg, 1977),
16. C.F. Bohren and D.R. Huffman, *Absorption and Scattering of Light by Small Particles*, (Wiley, New York, 1983).
17. L.G. Henyey and J.L. Greenstein, "Diffuse radiation in the galaxy," Astrophys. J. **93**, 70-83 (1941).
18. T.A.Germer. SCATMECH: Polarized Light Scattering C++ Class Library, http://physics.nist.gov/scatmech.
19. D.E. Barrick, "Rough surface scattering based on the specular point theory," IEEE Trans. Ant. Prop **AP-16**, 449-454 (1968).
20. K.E. Torrance and E.M. Sparrow, "Theory of off-specular reflection from roughened surfaces," J. Opt. Soc. Am. **57**, 1105-1114 (1967).
21. S.-M.F. Nee, R.V. Dewees, T.-W. Nee, L.F. Johnson, and M.B. Moran, "Slope distribution of a rough surface measured by transmission scattering and polarization," Appl. Opt. **39**, 1561-1569 (2000).
22. T.A. Germer and C.C. Asmail, "Goniometric optical scatter instrument for out-of-plane ellipsometry measurements," Rev. Sci. Instr. **70**, 3688-3695 (1999).
23. T.A. Germer and C.C. Asmail, "A goniometric optical scatter instrument for bidirectional reflectance distribution function measurements with out -of-plane and polarimetry capabilities," in *Scattering and Surface Roughness*, Z.-H. Gu and A.A. Maradudin, Eds., Proc. SPIE **3141**, 220-231, (1997)